

# Wireless Information and Power Transfer: Architecture Design and Rate-Energy Tradeoff

Xun Zhou, Rui Zhang, and Chin Keong Ho

## Abstract

Simultaneous information and power transfer over the wireless channels potentially offers great convenience to mobile users. Yet practical receiver designs impose technical constraints on its hardware realization, as practical circuits for harvesting energy from radio signals are not yet able to decode the carried information directly. To make theoretical progress, we propose a general receiver operation, namely, *dynamic power splitting* (DPS), which splits the received signal with adjustable power ratio for energy harvesting and information decoding, separately. Three special cases of DPS, namely, *time switching* (TS), *static power splitting* (SPS) and *on-off power splitting* (OPS) are investigated. The TS and SPS schemes can be treated as special cases of OPS. Moreover, we propose two types of practical receiver architectures, namely, *separated* versus *integrated* information and energy receivers. The integrated receiver integrates the front-end components of the separated receiver, thus achieving a smaller form factor. The rate-energy tradeoff for these two architectures are characterized by a so-called *rate-energy* (R-E) region. The optimal transmission strategy is derived to achieve different rate-energy tradeoffs. With receiver circuit power consumption taken into account, it is shown that the OPS scheme is optimal for both receivers. For the ideal case when the receiver circuit does not consume power, the SPS scheme is optimal for both receivers. In addition, we study the performance for the two types of receivers under a realistic system setup that employs practical modulation. Our results provide insights to the optimal practical receiver design for simultaneous wireless information and power transfer.

## Index Terms

Wireless power, wireless information and power transfer, rate-energy region, energy harvesting, circuit power.

## I. INTRODUCTION

Harvesting energy from the environment is a promising approach to prolong the lifetime of energy constrained wireless networks. Among other renewable energy sources such as solar and wind, background radio-frequency

This paper is to be presented in part at IEEE Global Communications Conference (Globecom), December 3-7, 2012, California, USA.

X. Zhou is with the Department of Electrical and Computer Engineering, National University of Singapore (e-mail:xunzhou@nus.edu.sg).

R. Zhang is with the Department of Electrical and Computer Engineering, National University of Singapore (e-mail:elezhang@nus.edu.sg).

He is also with the Institute for Infocomm Research, A\*STAR, Singapore.

C. K. Ho is with the Institute for Infocomm Research, A\*STAR, Singapore (e-mail:hock@i2r.a-star.edu.sg).

(RF) signals radiated by ambient transmitters can be a viable new source for wireless power transfer (WPT). On the other hand, RF signals have been widely used as a vehicle for wireless information transmission (WIT). Simultaneous wireless information and power transfer becomes appealing since it realizes both useful utilizations of RF signals at the same time, and thus potentially offers great convenience to mobile users.

Simultaneous information and power transfer over the wireless channels has been studied in [1]–[9]. Varshney first proposed the idea of transmitting information and energy simultaneously in [1]. A capacity-energy function was proposed to characterize the fundamental performance tradeoff for simultaneous information and power transfer. In [2], Grover and Sahai extended the work in [1] to frequency-selective channels with additive white Gaussian noise (AWGN). It was shown in [2] that a non-trivial tradeoff exists for information transfer versus energy transfer via power allocation. Wireless information and power transfer subject to co-channel interference was studied in [3], in which optimal designs to achieve different outage-energy tradeoffs as well as rate-energy tradeoffs are derived. Different from the traditional view of taking interference as an undesired factor that jeopardizes the wireless channel capacity, in [3] interference was utilized as a source for energy harvesting. Unlike [1]–[3], which considered point-to-point single-antenna transmission, [4]–[6] considered multiple-input multiple-output (MIMO) systems for simultaneous information and energy transfer. In particular, [4] studied the performance limits of a three-node MIMO broadcasting system, where one receiver harvests energy and another receiver decodes information from the signals sent by a common transmitter. [5] extended the work in [4] by considering imperfect channel state information (CSI) at the transmitter. MIMO relay systems involving an energy harvesting receiver were studied in [6], in which the joint optimal source and relay precoders were designed to achieve different tradeoffs between the energy transfer and the information rates. Simultaneous information and power transfer for multi-user systems was studied in [7]. It was shown in [7] that for multiple access channels with a received energy constraint, time-sharing is necessary to achieve the maximum sum-rate when the received energy constraint is sufficiently large; while for the multi-hop channel with a harvesting relay, the transmission strategy depends on the quality of the second link. Networks that involve wireless power transfer were studied in [8], [9]. In [8], the authors studied a hybrid network which overlays an uplink cellular network with randomly deployed power beacons that charge mobiles wirelessly. Under an outage constraint on the data links, the tradeoffs between the network parameters

were derived. In [9], the authors investigated a cognitive radio network powered by opportunistic wireless energy harvesting, where mobiles from the secondary network either harvest energy from nearby transmitters in a primary network, or transmit information if the primary transmitters are far away. Under an outage constraint for coexisting networks, the throughput of the secondary network was maximized.

Despite the recent interest in simultaneous information and power transfer, there remains two key challenges for practical implementations. First, it is assumed in [1], [2] that the receiver is able to observe and extract power simultaneously from the same received signal. However, this assumption may not hold in practice, as practical circuits for harvesting energy from radio signals are not yet able to decode the carried information directly. Due to this potential limitation, the results in [1], [2] actually provided only optimistic performance bounds. It thus motivates our investigation of novel practical receiver architectures to approach the performance bounds. Second, the conventional information receiver architecture designed for WIT may not be optimal for simultaneous information and power transfer, due to the fact that WIT and WPT operate with very different power sensitivity at the receiver (e.g., -10dBm for energy receivers versus -60dBm for information receivers). Thus, for a system that involves both WIT and WPT, the receiver architecture should be optimized for WPT. In addition, circuit power consumed by information decoding becomes a significant design issue for simultaneous information and power transfer, since the circuit power reduces the net harvested energy that can be stored in the battery for future use by the consumed energy. In particular, the active mixers used in conventional information receiver for RF to baseband conversion are substantially power-consuming. It thus motivates us to propose new receiver architectures which consume less power on down conversion by avoiding the use of active devices.

In this paper, we study practical receiver designs for a point-to-point wireless link with simultaneous information and power transfer (see Fig. 1). Due to the potential limitation for concurrent information and power transfer, we propose a general receiver operation scheme, namely, *dynamic power splitting* (DPS), by which the signal is dynamically split into two streams with arbitrary power ratio over time. Three special cases of DPS, namely, *time switching* (TS), *static power splitting* (SPS) and *on-off power splitting* (OPS) are investigated. The TS and SPS schemes can be treated as special cases of the OPS scheme. Based on DPS, we first consider the *separated* receiver architecture (see Fig. 4) based on a conventional information-decoding architecture. In this architecture,

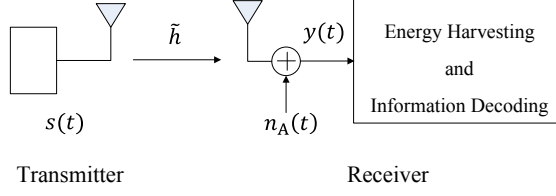


Fig. 1. System model.

the received signal by the antenna is split into two signal streams in the RF band, which are then separately fed to the conventional energy receiver and information receiver for harvesting energy and decoding information, respectively. Next, we propose an *integrated* receiver architecture (see Fig. 5), in which we integrate the information decoding and the energy harvesting circuits. In this architecture, the active RF band to baseband conversion in conventional information decoding is replaced by a passive rectifier operation, that is conventionally used only for energy harvesting. By providing a dual use of the rectifier, the energy cost for information decoding is reduced significantly.

The rate-energy performances for the two proposed receivers are further characterized by a so-called rate-energy (R-E) region. With receiver circuit power consumption taken into account, it is shown that the OPS scheme is optimal for both receivers. For the ideal case when the consumed power at the receiver is negligible, the SPS scheme is optimal for both receivers. Finally, the performance for the two receivers are compared under a realistic system setup that employs practical modulation. The results show that for a system with zero-net-energy consumption, the integrated receiver achieves more rate than separated receiver at sufficiently small transmission distance.

The rest of this paper is organized as follows: Section II presents the system model. Section III proposes the two receiver architectures. Section IV and Section V study the rate-energy performance for the separated and integrated receivers, respectively. Section VI extends the results in Sections IV and V to the case with receiver circuit power taken into consideration. Section VII studies the performance for the two types of receivers under a realistic system setup. Finally, Section VIII concludes the paper.

## II. SYSTEM MODEL

### A. Channel Model

As shown in Fig. 1, this paper studies a point-to-point wireless link with simultaneous information and power transfer. Both the transmitter and receiver are equipped with one single antenna. At the transmitter side, the complex baseband signal is expressed as  $x(t) = A(t)e^{j\phi(t)}$ , where  $A(t)$  and  $\phi(t)$  denote the amplitude and the phase of  $x(t)$ , respectively. It is assumed that  $x(t)$  is a narrow-band signal with bandwidth of  $B$  Hz, and  $\mathbb{E}[|x(t)|^2] = 1$ , where  $\mathbb{E}[\cdot]$  and  $|\cdot|$  denote the statistical expectation and the absolute value, respectively. The transmitted RF band signal is then given by  $s(t) = \sqrt{2P}A(t) \cos(2\pi ft + \phi(t)) = \sqrt{2P}\Re\{x(t)e^{j2\pi ft}\}$ , where  $P$  is the average transmit power, i.e.,  $\mathbb{E}[s^2(t)] = P$ ,  $f$  is the carrier frequency, and  $\Re\{\cdot\}$  denotes the real part of a complex number. It is assumed that  $B \ll f$ .

The transmitted signal propagates through a wireless channel with channel gain  $h > 0$  and phase shift  $\theta \in [0, 2\pi)$ . Thus, the signal arriving at the receiver can be expressed as  $s_h(t) = \sqrt{2hP}A(t) \cos(2\pi ft + \phi(t) + \theta) = \sqrt{2P}\Re\{\tilde{h}x(t)e^{j2\pi ft}\}$ , where  $\tilde{h} = \sqrt{h}e^{j\theta}$  denotes the equivalent complex channel.

Assuming that the receiving antenna operates at the same frequency band as the transmitted signal, the noise  $n_A(t)$  introduced by the receiving antenna can be modeled as a narrow-band (with bandwidth  $B$  and center frequency  $f$ ) Gaussian noise, i.e.,  $n_A(t) = \sqrt{2}\Re\{\tilde{n}_A(t)e^{j2\pi ft}\}$ , where  $\tilde{n}_A(t) = n_I(t) + jn_Q(t)$  with  $n_I(t)$  and  $n_Q(t)$  denoting the in-phase and quadrature noise components, respectively. We assume that  $n_I(t)$  and  $n_Q(t)$  are independent Gaussian random variables (RVs) with zero mean and variance  $\sigma_A^2/2$ , denoted by  $\mathcal{N}(0, \sigma_A^2/2)$ , where  $\sigma_A^2 = N_0B$ , and  $N_0$  is the one-sided noise power spectral density. Thus, we have  $\tilde{n}_A(t) \sim \mathcal{CN}(0, \sigma_A^2)$ , i.e.,  $\tilde{n}_A(t)$  is a circularly symmetric complex Gaussian (CSCG) RV with zero mean and variance  $\sigma_A^2$ .

Corrupted by the antenna noise, the received signal is expressed as  $y(t) = s_h(t) + n_A(t)$ . For convenience, we rewrite  $y(t)$  as  $y(t) = \sqrt{2}\Re\{\tilde{y}(t)\}$ , where the complex signal  $\tilde{y}(t)$  is

$$\tilde{y}(t) = \sqrt{hP}x(t)e^{j(2\pi ft + \theta)} + \tilde{n}_A(t)e^{j2\pi ft}. \quad (1)$$

### B. Information Receiver

First, we consider the case where the receiver shown in Fig. 1 is solely an information receiver, and review existing results on the traditional wireless information transfer system. Fig. 2 shows the standard operations at an

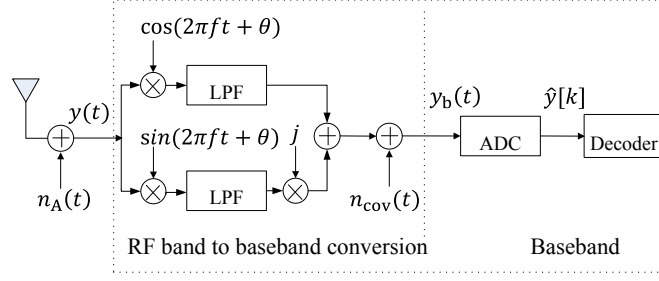


Fig. 2. Information receiver.

information receiver with coherent demodulation (assuming that the channel phase shift  $\theta$  is perfectly known at the receiver). The received RF band signal  $y(t)$  is first converted to a complex baseband signal  $y_b(t)$  by demodulation and low-pass filtering, which is equivalent to multiplying  $\tilde{y}(t)$  given in (1) by  $e^{-j(2\pi ft + \theta)}$ . Furthermore, by denoting  $n_{\text{cov}}(t)$  as the additive noise due to the above RF band to baseband signal conversion with  $n_{\text{cov}}(t) \sim \mathcal{CN}(0, \sigma_{\text{cov}}^2)$ ,  $y_b(t)$  is expressed as

$$\begin{aligned} y_b(t) &= \tilde{y}(t)e^{-j(2\pi ft + \theta)} + n_{\text{cov}}(t) \\ &= \sqrt{hP}x(t) + \tilde{n}_A(t)e^{-j\theta} + n_{\text{cov}}(t). \end{aligned} \quad (2)$$

Since  $\tilde{n}_A(t)e^{-j\theta}$  has the same distribution as  $\tilde{n}_A(t)$ , for convenience we use  $\tilde{n}_A(t)$  to denote  $\tilde{n}_A(t)e^{-j\theta}$  in the sequel. The baseband signal  $y_b(t)$  is then sampled and digitalized by an analog-to-digital converter (ADC) for further decoding. For simplicity, in this paper we assume an ideal ADC with zero quantization noise. Thus, from (2) the discrete-time ADC output is given by

$$\hat{y}[k] = \sqrt{hP}x[k] + \tilde{n}_A[k] + n_{\text{cov}}[k] \quad (3)$$

where  $k = 1, 2, \dots$ , denotes the symbol index.

It follows from (3) that the equivalent baseband channel for wireless information transmission is the well-known AWGN channel:

$$Y = \sqrt{hP}X + Z \quad (4)$$

where  $X$  and  $Y$  denote the channel input and output, respectively, and  $Z \sim \mathcal{CN}(0, \sigma_A^2 + \sigma_{\text{cov}}^2)$  denotes the complex Gaussian noise (assuming independent  $\tilde{n}_A(t)$  and  $n_{\text{cov}}(t)$ ). When the channel input is distributed as  $X \sim \mathcal{CN}(0, 1)$ ,

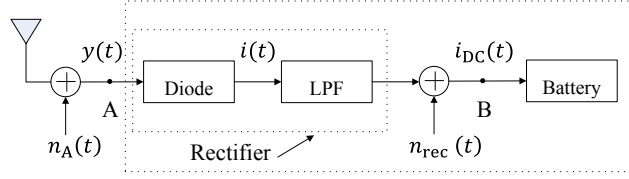


Fig. 3. Energy receiver.

the maximum achievable information rate (in bps/Hz) or the capacity of the AWGN channel is given by [10]

$$R = \log_2 \left( 1 + \frac{hP}{\sigma_A^2 + \sigma_{\text{cov}}^2} \right). \quad (5)$$

### C. Energy Receiver

Next, we consider the case where the receiver in Fig. 1 is solely an energy receiver, and derive the average wireless power that can be harvested from the received signal. Fig. 3 illustrates the operations of a typical energy receiver that converts RF energy directly via a *rectenna* architecture [11]. In the rectenna, the received RF band signal  $y(t)$  is converted to a direct current (DC) signal  $i_{\text{DC}}(t)$  by a rectifier, which consists of a Schottky diode and a passive low-pass filter (LPF). The DC signal  $i_{\text{DC}}(t)$  is then used to charge the battery to store the energy. With an input voltage proportional to  $y(t)$ , the output current  $i(t)$  of a Schottky diode is given by [12]:

$$i(t) = I_s \left( e^{\gamma y(t)} - 1 \right) = a_1 y(t) + a_2 y^2(t) + a_3 y^3(t) + \dots \quad (6)$$

where  $I_s$  denotes the saturation current,  $\gamma$  denotes the reciprocal of the thermal voltage of the Schottky diode, and the coefficients  $a_n$ 's are given by  $a_n = I_s \gamma^n / n!$ ,  $n = 1, 2, \dots$ , due to the Taylor series expansion of the exponential function.

From (1), for convenience we re-express  $y(t)$  as follows:

$$\begin{aligned} y(t) &= \sqrt{2} \Re \{ \sqrt{hP} x(t) e^{j(2\pi ft + \theta)} + \tilde{n}_A(t) e^{j2\pi ft} \} \\ &= \sqrt{2} \mu_Y(t) \cos(2\pi ft + \phi_Y(t)) \end{aligned} \quad (7)$$

where  $\phi_Y(t) = \arctan \frac{\mu_Q(t)}{\mu_I(t)}$  and

$$\mu_Y(t) = \sqrt{\mu_I^2(t) + \mu_Q^2(t)} \quad (8)$$

with

$$\mu_I(t) = \sqrt{hP}A(t) \cos(\phi(t) + \theta) + n_I(t) \quad (9)$$

$$\mu_Q(t) = \sqrt{hP}A(t) \sin(\phi(t) + \theta) + n_Q(t). \quad (10)$$

By substituting (7) into (6) and ignoring the higher-order (larger than two) terms of  $y(t)$ , we obtain

$$\begin{aligned} i(t) &\approx \sqrt{2}a_1\mu_Y(t) \cos(2\pi ft + \phi_Y(t)) + 2a_2\mu_Y^2(t) \cos^2(2\pi ft + \phi_Y(t)) \\ &= a_2\mu_Y^2(t) + \sqrt{2}a_1\mu_Y(t) \cos(2\pi ft + \phi_Y(t)) + a_2\mu_Y^2(t) \cos(4\pi ft + 2\phi_Y(t)). \end{aligned} \quad (11)$$

The output current  $i(t)$  of the diode is processed by a LPF, through which the high-frequency harmonic components at both  $f$  and  $2f$  in  $i(t)$  are removed and a DC signal  $i_{DC}(t)$  appears as the output of the rectifier. Assuming that the additive noise introduced by the rectifier is  $n_{rec}(t)$ , the filtered output  $I_{DC}(t)$  is thus given by

$$i_{DC}(t) = a_2\mu_Y^2(t) + n_{rec}(t). \quad (12)$$

Since  $a_2$  is a constant specified by the diode, for convenience we assume in the sequel that  $a_2 = 1$  (with  $n_{rec}(t)$  normalized accordingly to maintain the signal-to-noise ratio (SNR)). Note that in (12),  $a_2$  involves unit conversion from a power signal to a current signal, thus by normalization  $n_{rec}(t)$  can be equivalently viewed as a power signal. Assume  $n_{rec}(t) \sim \mathcal{N}(0, \sigma_{rec}^2)$ , where  $\sigma_{rec}$  is in watt. Substituting (8), (9) and (10) into (12) yields

$$i_{DC}(t) = \left( \sqrt{hP}A(t) \cos(\phi(t) + \theta) + n_I(t) \right)^2 + \left( \sqrt{hP}A(t) \sin(\phi(t) + \theta) + n_Q(t) \right)^2 + n_{rec}(t). \quad (13)$$

We assume that the converted power to be stored in the battery is linearly proportional to  $i_{DC}(t)$  [13], with a conversion efficiency  $0 < \zeta \leq 1$ . We also assume that the harvested power due to the noise (including both the antenna noise and the rectifier noise) is a small constant and thus ignored. Hence, the average power (normalized by the symbol period) stored in the battery, denoted by  $Q$  in watt or joule/sec, is given by

$$Q = \zeta \mathbb{E}[i_{DC}(t)] = \zeta hP. \quad (14)$$

#### D. Performance Upper Bound

Now consider the general case of interest where both information decoding and energy harvesting are implemented at the receiver, as shown in Fig. 1. Our main objective is to maximize both the decoded information rate  $R$



and harvested power  $Q$  from the same received signal  $y(t)$ . Based on the results in the previous two subsections, we derive an upper bound for the performance of any practical receiver with the joint operations of information decoding and energy harvesting, as follows. For information transfer, according to the data-processing inequality [10], with a given antenna noise  $\tilde{n}_A(t) \sim \mathcal{CN}(0, \sigma_A^2)$ , the maximum information rate  $R$  that can be reliably decoded at the receiver is upper-bounded by  $R \leq \log_2(1 + hP/\sigma_A^2)$ . Note that state-of-the-art wireless information receivers are not yet able to achieve this rate upper bound due to additional processing noise such as the RF band to baseband conversion noise  $n_{\text{cov}}(t)$ , as shown in (5). On the other hand, for energy transfer, according to the law of energy conservation, the maximum harvested power  $Q$  to be stored in the battery cannot be larger than that received by the receiving antenna, i.e.,  $Q \leq hP$ . Note that practical energy receivers cannot achieve this upper bound unless the energy conversion efficiency  $\zeta$  is made ideally equal to unity, as suggested by (14). Following the definition of rate-energy (R-E) region given in [1], [2], [4] to characterize all the achievable rate (in bps/Hz for information transfer) and energy (in joules/sec for energy transfer) pairs under a given transmit power constraint  $P$ , we obtain a performance upper bound on the achievable R-E region for the system in Fig. 1 as

$$\mathcal{C}_{\text{R-E}}^{\text{UB}}(P) \triangleq \left\{ (R, Q) : R \leq \log_2 \left( 1 + \frac{hP}{\sigma_A^2} \right), Q \leq hP \right\} \quad (15)$$

which is a box specified by three vertices  $(0, Q_{\max})$ ,  $(R_{\max}, 0)$  and  $(R_{\max}, Q_{\max})$ , with  $Q_{\max} = hP$  and  $R_{\max} = \log_2(1 + hP/\sigma_A^2)$ . Note that this performance bound is valid for all receiver architectures, as will be studied next.

### III. RECEIVER ARCHITECTURE FOR WIRELESS INFORMATION AND POWER TRANSFER

This section considers practical receiver designs for simultaneous wireless information and power transfer. We propose a general receiver operation called *dynamic power splitting* (DPS), from which we propose *separated* information and energy receiver and *integrated* information and energy receiver.

#### A. Dynamic Power Splitting

Currently, practical circuits for harvesting energy from radio signals are not yet able to decode the carried information directly. In other words, the signal that is used for harvesting energy cannot be reused for decoding information. Due to this potential limitation, we propose a practical DPS scheme to enable the receiver to harvest energy and decode information from the same received signal at any time  $t$ , by dynamically splitting the signal into

two streams with the power ratio  $\rho(t) : 1 - \rho(t)$ , which are used for harvesting energy and decoding information, respectively, where  $0 \leq \rho(t) \leq 1$ .

Consider a block-based transmission of duration  $T$  with  $T = NT_s$ , where  $N$  denotes the number of transmitted symbols per block and  $T_s$  denotes the symbol period. We assume that  $\rho(t) = \rho_k$  for any symbol interval  $t \in [(k-1)T_s, kT_s)$ ,  $k = 1, \dots, N$ . For convenience, we define a power splitting vector as  $\boldsymbol{\rho} = [\rho_1, \dots, \rho_N]^T$ . In addition, in this paper we assume an ideal power splitter at the receiver without any power loss or noise introduced, and that the receiver can perfectly synchronize its operations with the transmitter based on a given vector  $\boldsymbol{\rho}$ . During the transmission block time  $T$ , it is assumed that the information receiver may operate in two modes: switch off (off mode) for a time duration  $T_{\text{off}}$  to save power, or switch on (on mode) for a time duration  $T_{\text{on}} = T - T_{\text{off}}$  to decode information. The percentage of time that the information decoder operates in off mode is denoted by  $\alpha$  with  $0 \leq \alpha \leq 1$ , thus we have  $T_{\text{off}} = \alpha T$  and  $T_{\text{on}} = (1 - \alpha)T$ . Without loss of generality, we assume that the information receiver operates in off mode during the first  $\lfloor \alpha N \rfloor$  symbols during each block with  $k = 1, \dots, \lfloor \alpha N \rfloor$ , where  $\lfloor \cdot \rfloor$  denotes the floor operation, while in on mode during the remaining symbols with  $k = \lfloor \alpha N \rfloor + 1, \dots, N$ . For convenience, we also assume in the sequel that  $\alpha N$  is a positive integer regardless of the value of  $\alpha$ , which is approximately true if  $N$  is chosen to be a very large number in practice.

Next, we investigate three special cases of DPS, namely *time switching* (TS), *static power splitting* (SPS) and *on-off power splitting* (OPS) given in [4]:

- *Time switching (TS)*: With TS, for the first  $\alpha N$  symbols when the information receiver operates in off mode, all signal power is used for energy harvesting. For the remaining  $(1 - \alpha)N$  symbols when the information receiver operates in on mode, all signal power is used for energy harvesting. Thus for TS, we have

$$\rho_k = \begin{cases} 1, & k = 1, \dots, \alpha N \\ 0, & k = \alpha N + 1, \dots, N. \end{cases} \quad (16)$$

- *Static power splitting (SPS)*: With SPS, the information receiver operates in on mode for all  $N$  symbols, i.e.,  $\alpha = 0$ . Moreover, the ratio of the split signal power for harvesting energy and decoding information is set to be a constant  $\rho$  for all  $N$  symbols. Thus for SPS, we have

$$\rho_k = \rho, \quad k = 1, \dots, N. \quad (17)$$

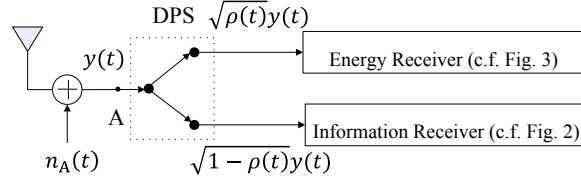


Fig. 4. Architecture for the separated information and energy receiver.

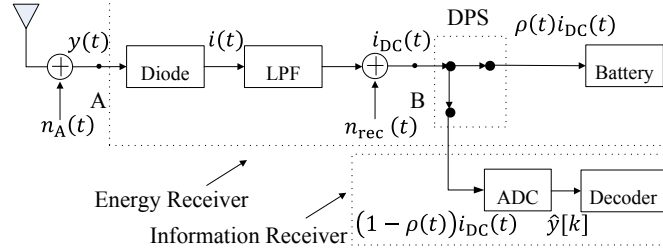


Fig. 5. Architecture for the integrated information and energy receiver.

- *On-off power splitting (OPS)*: With OPS, for the first  $\alpha N$  symbols all signal power is used for energy harvesting. For the remaining  $(1 - \alpha)N$  symbols, the ratio of the split signal power for harvesting energy and decoding information is set to be a constant  $\rho$ , with  $0 \leq \rho < 1$ . Thus, for a given power splitting pair  $(\alpha, \rho)$ , we have

$$\rho_k = \begin{cases} 1, & k = 1, \dots, \alpha N \\ \rho, & k = \alpha N + 1, \dots, N. \end{cases} \quad (18)$$

Note that TS and SPS are two special cases of OPS by letting  $\rho = 0$  (for TS) or  $\alpha = 0$  (for SPS) in (18).

### B. Separated vs. Integrated Receivers

In this subsection, we propose two types of receivers that exploit the DPS scheme in different ways. One type of receivers is called *separated* information and energy receiver, as shown in Fig. 4, while the other is called *integrated* information and energy receiver, as shown in Fig. 5. Note that these two types of receivers both use the energy receiver in Fig. 3 for energy harvesting; however, their difference lies in that for the case of separated receiver, the power splitter for DPS is inserted at point ‘A’ in the RF band of the energy receiver shown in Fig. 3, while in the case of integrated receiver, the power splitter is inserted at point ‘B’ in the baseband.

First, we consider the case of separated information and energy receiver. As shown in Fig. 4, a power splitter is inserted at point ‘A’, such that the received signal  $y(t)$  by the antenna is split into two signal streams with

power levels specified by  $\rho(t)$  in the RF band, which are then separately fed to the conventional energy receiver (cf. Fig. 3) and information receiver (cf. Fig. 2) for harvesting energy and decoding information, respectively. The achievable R-E region for this type of receivers with DPS will be studied in Section IV.

Next, we consider the integrated information and energy receiver, as motivated by the following key observation. Since the transmitted power in a wireless power transfer system can be varied over time provided that the average power delivered to the receiver is above a certain required target, we can encode information in the energy signal by varying its power levels over time, thus achieving continuous information transfer without degrading the power transfer efficiency. Similar to the conventional digital modulation techniques, whereby information is modulated on a carrier signal in the RF band by varying its amplitude, phase, and/or frequency, this new type of modulation scheme by exploiting the energy domain is thus called *energy modulation*. Note that to decode the energy modulated information at the receiver, we need to detect the power variation in the received signal within a certain accuracy, by applying techniques such as *energy detection* [14]. Recall that in Section II-C, for the energy receiver in Fig. 3, the received RF signal  $y(t)$  is converted to a DC signal  $i_{\text{DC}}(t)$  given in (13) by a rectifier. Note that this RF to DC conversion is analogous to the RF band to baseband conversion in conventional wireless information receivers in Fig. 2. Thus,  $i_{\text{DC}}(t)$  can be treated as a baseband signal for information decoding (via energy detection).

Based on the above observation, we propose the integrated information and energy receiver as shown in Fig. 5, by inserting a power splitter at point ‘B’ of the conventional energy receiver. With DPS,  $i_{\text{DC}}(t)$  is split into two portions specified by  $\rho(t)$  for energy harvesting and information decoding, respectively. Note that unlike the traditional information receiver in Fig. 2, the information receiver in the case of integrated receiver does not implement any RF band to baseband conversion, since this operation has been *integrated* to the energy receiver (via the rectifier). The achievable R-E region for this type of receivers will be studied in Section V.

#### IV. RATE-ENERGY TRADEOFF FOR SEPARATED INFORMATION AND ENERGY RECEIVER

In this section, we study the achievable R-E region for the separated information and energy receiver shown in Fig. 4. With DPS, the average SNR at the information receiver for the  $k$ -th transmitted symbol,  $k = 1, \dots, N$ , is denoted by  $\tau(\rho_k)$ , and given by

$$\tau(\rho_k) = \frac{(1 - \rho_k)hP}{(1 - \rho_k)\sigma_A^2 + \sigma_{\text{cov}}^2}. \quad (19)$$

From (19), we obtain the achievable R-E region for the DPS scheme in the case of separated receiver as

$$\mathcal{C}_{\text{R-E}}^{\text{DPS}}(P) \triangleq \bigcup_{\rho} \left\{ (R, Q) : Q \leq \frac{1}{N} \sum_{k=1}^N \rho_k \zeta h P, \quad R \leq \frac{1}{N} \sum_{k=1}^N \log_2 \left( 1 + \frac{(1 - \rho_k) h P}{(1 - \rho_k) \sigma_A^2 + \sigma_{\text{cov}}^2} \right) \right\}. \quad (20)$$

Next, we address the two special cases of DPS, i.e., the TS scheme and the SPS scheme. Substituting (16) into (20), the achievable R-E region for the TS scheme is given by

$$\mathcal{C}_{\text{R-E}}^{\text{TS}}(P) \triangleq \bigcup_{\alpha} \left\{ (R, Q) : Q \leq \alpha \zeta h P, \quad R \leq (1 - \alpha) \log_2 \left( 1 + \frac{h P}{\sigma_A^2 + \sigma_{\text{cov}}^2} \right) \right\}. \quad (21)$$

Let  $\hat{R}_{\text{max}} = \log_2 (1 + h P / (\sigma_A^2 + \sigma_{\text{cov}}^2))$  given in (5) and  $\hat{Q}_{\text{max}} = \zeta h P$  given in (14). It is noted that the boundary of  $\mathcal{C}_{\text{R-E}}^{\text{TS}}(P)$  is simply a straight line connecting the two points  $(\hat{R}_{\text{max}}, 0)$  and  $(0, \hat{Q}_{\text{max}})$  as  $\alpha$  sweeps from 0 to 1.

Substituting (17) into (20), the achievable R-E region for the SPS scheme is given by

$$\mathcal{C}_{\text{R-E}}^{\text{SPS}}(P) \triangleq \bigcup_{\rho} \left\{ (R, Q) : Q \leq \rho \zeta h P, \quad R \leq \log_2 \left( 1 + \frac{(1 - \rho) h P}{(1 - \rho) \sigma_A^2 + \sigma_{\text{cov}}^2} \right) \right\}. \quad (22)$$

**Proposition 4.1:** For the separated information and energy receiver, the SPS scheme is the optimal DPS scheme,

i.e.,  $\mathcal{C}_{\text{R-E}}^{\text{DPS}}(P) = \mathcal{C}_{\text{R-E}}^{\text{SPS}}(P), \forall P \geq 0$ .

*Proof:* Please refer to Appendix A. ■

From Proposition 4.1, it suffices for us to consider the SPS scheme for the optimal R-E tradeoff in the case of separated receivers. In particular, if  $\sigma_A^2 \ll \sigma_{\text{cov}}^2$ , i.e., the processing noise is dominant over the antenna noise, from (19) the SNR at the information receiver  $\tau(\rho) \rightarrow (1 - \rho) h P / \sigma_{\text{cov}}^2$ . In this case, it can be shown that  $\mathcal{C}_{\text{R-E}}^{\text{SPS}}(P) \rightarrow \mathcal{C}_{\text{R-E}}^{\text{TS}}(P)$ . In the other extreme case with  $\sigma_A^2 \gg \sigma_{\text{cov}}^2$ , from (19) we have  $\tau(\rho) \rightarrow h P / \sigma_A^2$ , which is independent of  $\rho$ . Thus, the optimal rate-energy tradeoff is achieved when infinitesimally small power is split to the information receiver, i.e.,  $\rho \rightarrow 1$ . In this case, it can be shown that when  $\zeta = 1$ ,  $\mathcal{C}_{\text{R-E}}^{\text{SPS}}(P) \rightarrow \mathcal{C}_{\text{R-E}}^{\text{UB}}(P)$ , which is the R-E tradeoff outer bound given in (15).

Fig. 6 shows the achievable R-E regions under different noise power setups for the separated information and energy receiver (SepRx). It is assumed that  $h = 1$ ,  $P = 100$ ,  $\zeta = 1$ , and the antenna noise power is set to be  $\sigma_A^2 = 1$ . With normalization, for convenience we denote the information rate and harvested energy in terms of bits/channel use and energy unit, respectively. In Fig. 6, it is observed that for SepRx, the SPS scheme always achieves larger R-E pairs than the TS scheme for different values of the processing (RF band to baseband conversion) noise power  $\sigma_{\text{cov}}^2$ . Moreover, as  $\sigma_{\text{cov}}^2$  increases, the gap between  $\mathcal{C}_{\text{R-E}}^{\text{TS}}(P)$  and  $\mathcal{C}_{\text{R-E}}^{\text{SPS}}(P)$  shrinks, while as  $\sigma_{\text{cov}}^2$  decreases, the

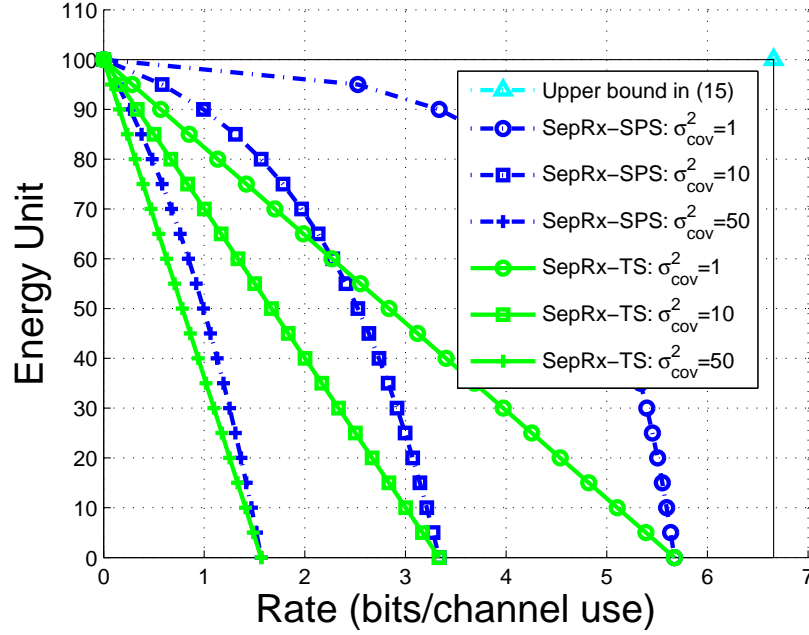


Fig. 6. Rate-energy tradeoff for TS vs. SPS based separated receiver with  $h = 1$ ,  $P = 100$ ,  $\zeta = 1$  and  $\sigma_A^2 = 1$ .

achievable R-E region with SPS enlarges and will eventually approach to the R-E region upper bound given in (15) when  $\sigma_{\text{cov}}^2 \rightarrow 0$ .

## V. RATE-ENERGY TRADEOFF FOR INTEGRATED INFORMATION AND ENERGY RECEIVER

In this section, we study the rate-energy performance for the integrated information and energy receiver shown in Fig. 5. From (13), for convenience we re-express  $i_{\text{DC}}(t)$  as follows:

$$i_{\text{DC}}(t) = \left| \sqrt{hP}A(t)e^{j(\theta+\phi(t))} + \tilde{n}_A(t) \right|^2 + n_{\text{rec}}(t). \quad (23)$$

Since planar rotation does not change the statistics of  $\tilde{n}_A(t)$ , (23) can be further written as

$$i_{\text{DC}}(t) = \left| \sqrt{hP}A(t) + \tilde{n}_A(t) \right|^2 + n_{\text{rec}}(t). \quad (24)$$

As shown in Fig. 5, after the noiseless power splitter and ADC, the output  $\hat{y}[k]$  is given by

$$\hat{y}[k] = (1 - \rho_k) \left( \left| \sqrt{hP}A[k] + \tilde{n}_A[k] \right|^2 + n_{\text{rec}}[k] \right), \quad k = 1, \dots, N. \quad (25)$$

In the above it is worth noting that the average SNR at any  $k$  is independent of  $\rho_k$  provided that  $\rho_k < 1$ . Thus, to minimize the power split for information decoding (or maximize the power split for energy harvesting), we should

let  $\rho_k \rightarrow 1, \forall k$ , i.e., splitting infinitesimally small power to the information receiver all the time. Thereby, DPS becomes an equivalent SPS with  $\rho \rightarrow 1$  in the case of integrated receiver.

With  $\rho_k$ 's all equal to 1 in (25), the equivalent discrete-time memoryless channel for the information decoder is modeled as

$$Y = \left| \sqrt{hPX} + Z_2 \right|^2 + Z_1 \quad (26)$$

where  $X$  denotes the signal power, which is the nonnegative channel input;  $Y$  denotes the channel output;  $Z_2 \sim \mathcal{CN}(0, \sigma_A^2)$  denotes the antenna noise; and  $Z_1 \sim \mathcal{N}(0, \sigma_{\text{rec}}^2)$  denotes the rectifier noise. It is worth noting that for the channel (26) information is encoded in the power (amplitude) of the transmitted signal  $x(t)$ , rather than the phase of  $x(t)$ . The channel in (26) is nonlinear and thus it is challenging to determine its capacity  $C_{\text{NL}}$  and corresponding optimal input distribution subject to  $X \geq 0$  and  $\mathbb{E}[X] \leq 1$ , where  $X$  is real. Similar to the case of separated receiver, we consider the following two special noise power setups:

- Case 1 (Dominant Rectifier Noise) with  $\sigma_A^2 \ll \sigma_{\text{rec}}^2$ : In this case, the rectifier noise is dominant over the antenna noise; thus,  $Z_2 \rightarrow 0$ . The channel in (26) becomes

$$Y = hPX + Z_1 \quad (27)$$

where  $X \geq 0$  and real-valued, which is known as the *optical intensity channel*. It is shown in [16] that the optimal input distribution to this channel is discrete. According to [17], the capacity  $C_1$  for the channel (27) is upper-bounded by

$$\begin{aligned} C_1^{\text{ub}} = & \left( \frac{1}{2} \mathcal{Q} \left( \frac{\delta}{\sigma_{\text{rec}}} \right) + \frac{\delta e^{-\frac{\delta^2}{2\sigma_{\text{rec}}^2}}}{2\sqrt{2\pi}\sigma_{\text{rec}}} + \frac{\delta^2}{2\sigma_{\text{rec}}^2} \left( 1 - \mathcal{Q} \left( \frac{\delta + hP}{\sigma_{\text{rec}}} \right) \right) + \frac{1}{\beta} \left( \delta + hP + \frac{\sigma_{\text{rec}} e^{-\frac{\delta^2}{2\sigma_{\text{rec}}^2}}}{\sqrt{2\pi}} \right) \right) \log_2 e \\ & + \log_2 \left( \beta e^{-\frac{\delta^2}{2\sigma_{\text{rec}}^2}} + \sqrt{2\pi}\sigma_{\text{rec}} \mathcal{Q} \left( \frac{\delta}{\sigma_{\text{rec}}} \right) \right) - \frac{1}{2} \log_2 2\pi e \sigma_{\text{rec}}^2 \end{aligned} \quad (28)$$

where  $\beta > 0$ ,  $\delta \geq 0$  are free parameters and  $\mathcal{Q}(\cdot) = \frac{1}{\sqrt{2\pi}} \int_x^\infty e^{-\frac{t^2}{2}} dt$  denotes the  $Q$ -function. Moreover, the asymptotic capacity at high power ( $P \rightarrow \infty$ ) is given by [17]

$$C_1^\infty = \log_2 \frac{hP}{\sigma_{\text{rec}}} + \frac{1}{2} \log_2 \frac{e}{2\pi}. \quad (29)$$

- Case 2 (Dominant Antenna Noise) with  $\sigma_A^2 \gg \sigma_{\text{rec}}$ : In this case, the antenna noise is dominant; thus,  $Z_1 \rightarrow 0$ .

The channel in (26) is then simplified as

$$Y = \left| \sqrt{hPX} + Z_2 \right|^2 \quad (30)$$

which is equivalent as the *noncoherent AWGN channel*. It is shown in [18] that the optimal input distribution to this channel is discrete and possesses an infinite number of mass points. The capacity  $C_2$  for the channel (30) is upper-bounded by [18]

$$C_2^{\text{ub}} = \frac{1}{2} \log_2 \left( 1 + \frac{hP}{\sigma_A^2} \right) + \frac{1}{2} \left( \log_2 \frac{2\pi}{e} - C_E \log_2 e \right) \quad (31)$$

where  $C_E$  is Euler's constant. Moreover, the asymptotic capacity at high power ( $P \rightarrow \infty$ ) is given by [18], [19]

$$C_2^\infty = \frac{1}{2} \log_2 \left( 1 + \frac{hP}{2\sigma_A^2} \right) \quad (32)$$

which is achieved by choosing  $X$  as central chi-square distribution with one degree of freedom<sup>1</sup>.

In general, the capacity  $C_{\text{NL}}$  of the channel given in (26) can be upper-bounded by

$$C_{\text{NL}}^{\text{ub}} = \min\{C_1^{\text{ub}}, C_2^{\text{ub}}\} \quad (33)$$

and the capacity lower bound  $C_{\text{NL}}^{\text{lb}}$  for the channel (26) can be computed by the mutual information obtained from any input distribution satisfying the constraint  $X \geq 0$  and  $\mathbb{E}[X] \leq 1$ . It is worth noting that at high power ( $P \rightarrow \infty$ ) from (29) and (32),  $C_1^\infty$  grows like  $\log_2 P$ ; while  $C_2^\infty$  grows like  $\frac{1}{2} \log_2 P$ . Thus the channel (30) provides a tighter upper bound for the asymptotic capacity of the channel (26) than the channel (27) at high SNR.

Fig. 7 shows the capacity bounds for the above three channels (26), (27) and (30). It is assumed that  $h = 1$ ,  $\sigma_A^2 = 10^{-4}$  and  $\sigma_{\text{rec}} = 1$ . The capacity lower bound  $C_{\text{NL}}^{\text{lb}}$  for the channel given in (26) is computed by assuming the input (power) as central chi-square distribution with one degree of freedom. It is observed that in this case with dominant rectifier noise, the capacity upper bound  $C_1^{\text{ub}}$  in (28) is tighter than  $C_2^{\text{ub}}$  in (31). It is also observed that the gap between the capacity upper and lower bounds, namely  $C_{\text{NL}}^{\text{ub}}$  and  $C_{\text{NL}}^{\text{lb}}$ , is still notably large under this setup, which can be further reduced by optimizing the input distribution.

<sup>1</sup>In this case, the input amplitude is distributed as the positive normal distribution, with probability density function  $f_A(a) = \sqrt{\frac{2}{\pi}} e^{-\frac{a^2}{2}}$ .



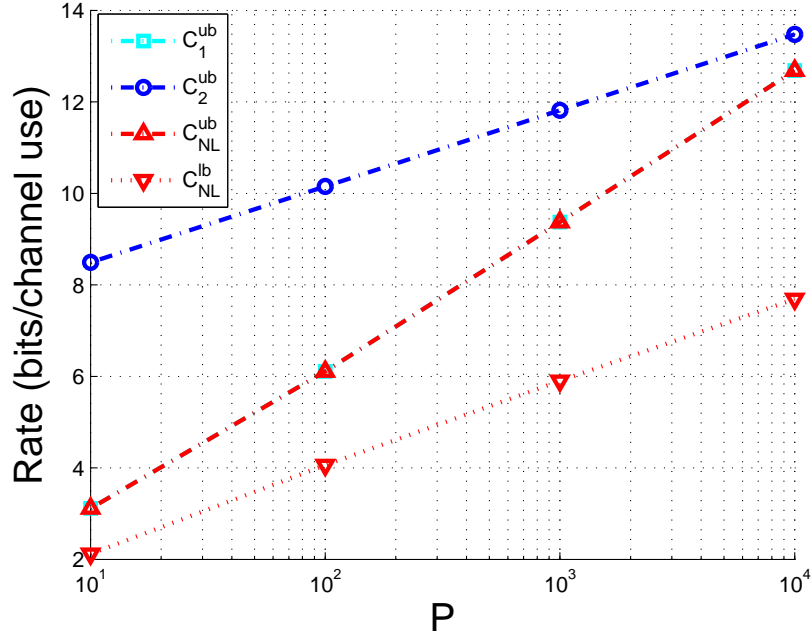


Fig. 7. Capacity bounds for the channels (26), (27) and (30) with  $h = 1$ ,  $\sigma_A^2 = 10^{-4}$  and  $\sigma_{\text{rec}} = 1$ .

To summarize, the achievable R-E region for the case of integrated receivers by SPS with  $\rho \rightarrow 1$  is given by

$$\mathcal{C}_{\text{R-E}}^{\text{SPS}}(P) \triangleq \{(R, Q) : R \leq C_{\text{NL}}(P), Q \leq \zeta h P\} \quad (34)$$

where  $C_{\text{NL}}(P)$  denotes the capacity of the nonlinear (NL) channel given in (26) subject to  $\mathbb{E}[X^2] \leq 1$ .

Fig. 8 shows the achievable R-E regions under different noise power setups for both cases of SepRx and IntRx. The achievable rates for IntRx are computed as the capacity lower bound for the channel given in (26) assuming the input as central chi-square distribution with one degree of freedom. As shown in Fig. 8, the achievable R-E regions for IntRx are marked by boxes as given in (34). In addition, when the processing noise power ( $\sigma_{\text{cov}}^2$  for SepRx and  $\sigma_{\text{rec}}$  for IntRx) equals to the antenna noise power, i.e.,  $\sigma_A^2 = \sigma_{\text{cov}}^2 = \sigma_{\text{rec}} = 1$ , the achievable rate for IntRx is notably lower than that for SepRx, due to the use of noncoherent (energy) modulation by IntRx as compared to the use of coherent modulation by SepRx. However, when the processing noise power is much greater than the antenna noise power (as in most practical systems), the achievable R-E region of IntRx becomes superior compared to that of SepRx with the same processing noise power, i.e.,  $\sigma_{\text{cov}}^2 = \sigma_{\text{rec}} = 100$ . This is due to the facts that for IntRx, the processing (rectifier) noise incurs prior to the power splitter and thus only infinitesimally small power is required to be split by the power splitter to implement the energy detection for information decoding (cf.

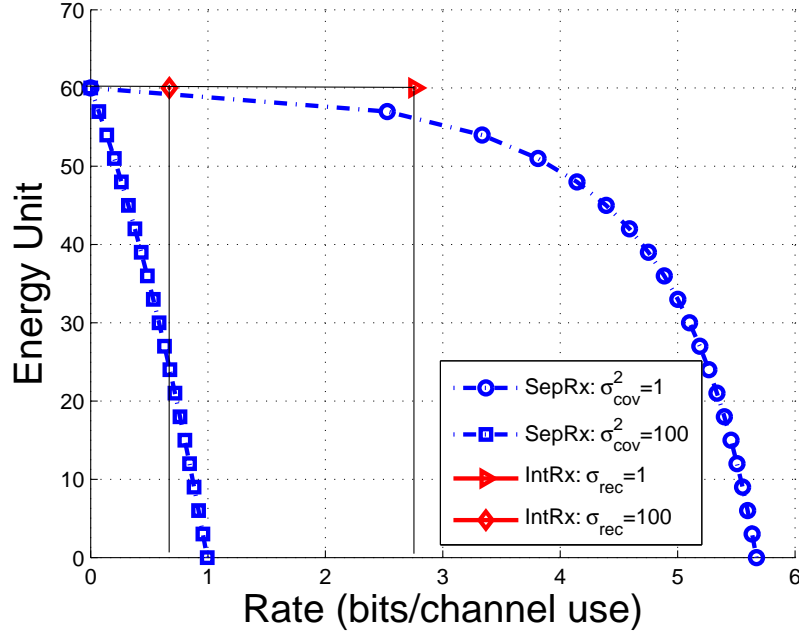


Fig. 8. Rate-energy tradeoff for separated vs. integrated receivers with  $h = 1$ ,  $P = 100$ ,  $\zeta = 0.6$  and  $\sigma_A^2 = 1$ .

(26)), while for SepRx, more substantial power needs to be split to the information decoder to compensate for the processing (RF band to baseband conversion) noise that incurs after the power splitter. Moreover, in Fig. 8 it is observed that IntRx is more suitable than SepRx when more wireless power is desired.

## VI. RATE-ENERGY TRADEOFF WITH RECEIVER CIRCUIT POWER CONSUMPTION

In Sections IV and V, the harvested power is characterized as the power harvested by the energy receiver without consideration of power consumption by the receiver circuits. For energy receiver, there is no energy consumption since both the Schottky diode and LPF are passive devices<sup>2</sup>. However, for information receiver, some amount of power will be consumed to supply the information decoding circuits. In particular, for the separated receiver shown in Fig. 4, the circuit power consumed by information decoding, denoted by  $P_S$ , is given by  $P_S = P_m + P_{ADC}$ , where  $P_m$  and  $P_{ADC}$  denote the power consumed by the RF band mixer and the ADC, respectively. For the integrated receiver shown in Fig. 5, however, the circuit power consumed by information decoding, denoted by  $P_I$ , is only given by  $P_I = P_{ADC}$ . Note that in general  $P_S$  will be much greater than  $P_I$ , since the RF band mixer consumes much more power than the ADC. Thus the *net energy* stored in the battery will be the harvested energy

<sup>2</sup>In practice, some RF energy harvesting systems have additional control circuits which consume power, however, this power consumption has been included in the conversion efficiency  $\zeta$

subtracted by that consumed by information decoding circuits. In this section, we study the rate-energy tradeoff for both separated and integrated receivers with receiver circuit power consumption taken into account.

#### A. Separated Receiver with $P_S > 0$

For the separated receiver shown in Fig. 4, by slightly modifying (20), the achievable R-E region for the DPS scheme is given by

$$\mathcal{C}_{R-E}^{\text{DPS}'}(P) \triangleq \bigcup_{\rho} \left\{ (R, Q) : Q \leq \frac{1}{N} \left( \sum_{k=1}^N \rho_k \zeta h P - \sum_{k=\alpha N+1}^N P_S \right), \right. \\ \left. R \leq \frac{1}{N} \sum_{k=\alpha N+1}^N \log_2 \left( 1 + \frac{(1-\rho_k)hP}{(1-\rho_k)\sigma_A^2 + \sigma_{\text{cov}}^2} \right) \right\}. \quad (35)$$

Next, we address one special case of DPS, i.e., the OPS scheme. Substituting (18) into (35), the achievable R-E region for the OPS scheme is given by

$$\mathcal{C}_{R-E}^{\text{OPS}'}(P) \triangleq \bigcup_{\alpha, \rho} \left\{ (R, Q) : Q \leq \alpha \zeta h P + (1-\alpha) \rho \zeta h P - (1-\alpha) P_S, \right. \\ \left. R \leq (1-\alpha) \log_2 \left( 1 + \frac{(1-\rho)hP}{(1-\rho)\sigma_A^2 + \sigma_{\text{cov}}^2} \right) \right\}. \quad (36)$$

**Proposition 6.1:** For the separated information and energy receiver with  $P_S > 0$ , the OPS scheme is the optimal DPS scheme, i.e.,  $\mathcal{C}_{R-E}^{\text{DPS}'}(P) = \mathcal{C}_{R-E}^{\text{OPS}'}(P), \forall P \geq 0$ .

*Proof:* Please refer to Appendix B. ■

From Proposition 6.1, it suffices to consider the OPS scheme for the optimal R-E tradeoff in the case of separated receivers. Unlike the case of  $P_S = 0$ , where the boundary of  $\mathcal{C}_{R-E}^{\text{DPS}} = \mathcal{C}_{R-E}^{\text{SPS}}$  is achieved as  $\rho$  sweeps from 0 to 1, the optimal power splitting pairs  $(\alpha^*, \rho^*)$  that achieve the boundary of  $\mathcal{C}_{R-E}^{\text{DPS}'} = \mathcal{C}_{R-E}^{\text{OPS}'}$  is to be determined. We thus consider the following optimization problem:

$$\begin{aligned} (\text{P0}) : \quad & \max_{\alpha, \rho} \quad R = (1-\alpha) \log_2 \left( 1 + \frac{(1-\rho)hP}{(1-\rho)\sigma_A^2 + \sigma_{\text{cov}}^2} \right) \\ & \text{s.t.} \quad \alpha \zeta h P + (1-\alpha) \rho \zeta h P - (1-\alpha) P_S \geq Q, \\ & \quad \quad 0 \leq \alpha \leq 1, \quad 0 \leq \rho \leq 1, \end{aligned}$$

The optimal solution of (P0) is obtained with the first constraint strictly equal, otherwise we can always decrease

$\alpha$  or  $\rho$  to obtain a larger rate  $R$ . Thus the boundary points  $(R, Q)$  satisfy the following two equations,

$$Q = \alpha \zeta h P + (1 - \alpha) \rho \zeta h P - (1 - \alpha) P_S, \quad (37)$$

$$R = (1 - \alpha) \log_2 \left( 1 + \frac{(1 - \rho) h P}{(1 - \rho) \sigma_A^2 + \sigma_{\text{cov}}^2} \right). \quad (38)$$

When  $\alpha = 1$ , we have  $(R, Q) = (0, \zeta h P)$ ; while  $0 \leq \alpha < 1$ , from (37), we have

$$\rho = \frac{Q - \alpha \zeta h P + (1 - \alpha) P_S}{(1 - \alpha) \zeta h P}. \quad (39)$$

Substituting (39) to (38), we have

$$R = (1 - \alpha) \log_2 \left( 1 + \frac{\frac{\zeta h P - Q - (1 - \alpha) P_S}{\zeta h P}}{\frac{\zeta h P - Q - (1 - \alpha) P_S}{\zeta h P} \sigma_A^2 + \sigma_{\text{cov}}^2 (1 - \alpha)} \right). \quad (40)$$

From (40),  $R$  is a function of  $\alpha$  with fixed  $Q$ . For convenience, we rewrite (40) as follows:

$$R(s) = s \log_2 \left( 1 + \frac{cs + d}{as + b} \right) \quad (41)$$

where  $s = 1 - \alpha$ ,  $a = \sigma_{\text{cov}}^2 - \frac{\sigma_A^2 P_S}{\zeta h P}$ ,  $b = \sigma_A^2 \left( 1 - \frac{Q}{\zeta h P} \right)$ ,  $c = -\frac{P_S}{\zeta}$  and  $d = h P \left( 1 - \frac{Q}{\zeta h P} \right)$ . Note that the feasible range of  $s$  is given by  $\frac{d}{h P - c} \leq s < \min\{-\frac{d}{c}, 1\}$  to ensure that  $0 \leq \alpha \leq 1$  and  $0 \leq \rho \leq 1$ .

The following lemma describes the behavior of  $R(s)$  in terms of  $s$ , which is important for determining the boundary points  $(R, Q)$ .

**Lemma 6.1:** Setting  $Q$  as a constant harvested power  $Q = q \in [0, \zeta h P]$ ,  $R(s)$  is concave in  $s \in [0, -\frac{d}{c}]$ .

Moreover, as  $s$  increases from 0 to  $-\frac{d}{c}$ ,  $R(s)$  decreases after an initial increase.

*Proof:* Please refer to Appendix C. ■

With Lemma 6.1, we have the following corollary for determination of the boundary points of  $\mathcal{C}_{\text{R-E}}^{\text{OPS}'}$ .

**Corollary 6.1:** Each boundary point  $(R, Q)$  of  $\mathcal{C}_{\text{R-E}}^{\text{OPS}'}$  is achieved by an unique optimal power splitting pair  $(\alpha^*, \rho^*)$ . For a given  $Q = q \in [0, \zeta h P]$ , the corresponding  $(\alpha^*, \rho^*)$  can be obtained by the following procedures

- Set  $Q = q$ , using bisection method to search the maximum value of  $R(s)$  for  $s \in [0, -\frac{d}{c}]$  and corresponding  $s = s^* \in [0, -\frac{d}{c}]$ .
- Corresponding  $(\alpha^*, \rho^*)$  at  $Q = q$  is given by

$$\alpha^* = \begin{cases} 1 - \frac{d}{h P - c}, & \text{if } 0 \leq s^* \leq \frac{d}{h P - c} \\ 1 - s^*, & \text{if } \frac{d}{h P - c} < s^* < 1 \\ 0, & \text{if } s^* \geq 1. \end{cases} \quad (42)$$

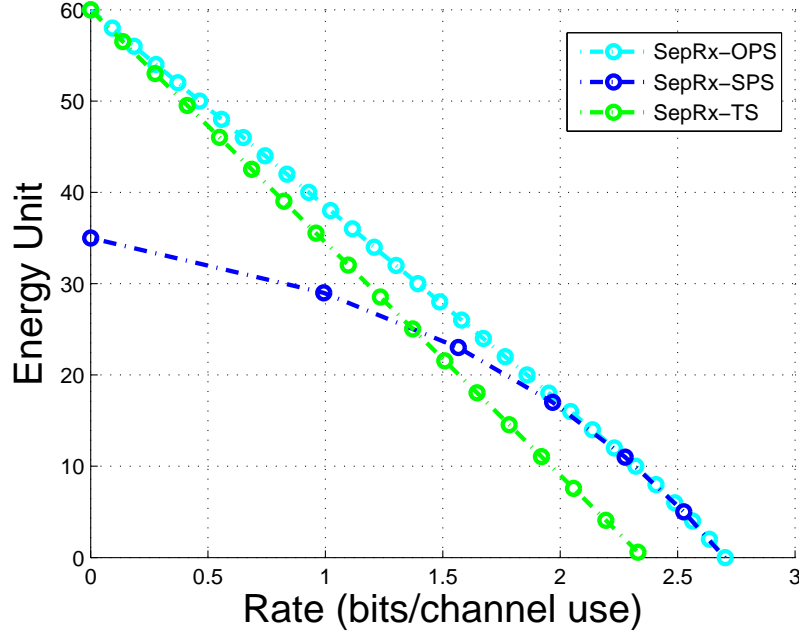


Fig. 9. Rate-energy tradeoff for the separated receiver with receiver circuit power consumption. It is assumed that  $h = 1$ ,  $P = 100$ ,  $\zeta = 0.6$ ,  $\sigma_A^2 = 1$ ,  $\sigma_{\text{cov}}^2 = 10$  and  $P_S = 25$ .

$\rho^*$  is given by (39) with  $Q = q$  and  $\alpha = \alpha^*$ .

- Corresponding  $R$  at  $Q = q$  is given by (38) with  $\alpha = \alpha^*$  and  $\rho = \rho^*$ .

*Proof:* Corollary 6.1 follows immediately from Lemma 6.1. ■

Fig. 9 shows the achievable R-E regions for SepRx with receiver circuit power consumption. For SepRx with  $P_S = 20$ , it is observed that  $\mathcal{C}_{R-E}^{\text{TS}'} \subseteq \mathcal{C}_{R-E}^{\text{OPS}'}$  and  $\mathcal{C}_{R-E}^{\text{SPS}'} \subseteq \mathcal{C}_{R-E}^{\text{OPS}'}$ . Moreover, SPS achieves the RE-region boundary only at low harvested power region, where  $\mathcal{C}_{R-E}^{\text{SPS}'}$  and  $\mathcal{C}_{R-E}^{\text{OPS}'}$  partially coincide. However, the performance of SPS becomes worse (even worse than TS) when more harvested power is desired, since it is unwise and energy-inefficient to keep information receiver always on during the whole transmission time.

### B. Integrated Receiver with $P_I > 0$

For the integrated receiver shown in Fig. 5, the achievable R-E region for the DPS scheme is given by

$$\mathcal{C}_{R-E}^{\text{DPS}'}(P) \triangleq \bigcup_{\rho} \left\{ (R, Q) : Q \leq \frac{1}{N} \left( \sum_{k=1}^N \rho_k \zeta h P - \sum_{k=\alpha N+1}^N P_I \right), R \leq \frac{1}{N} \sum_{k=\alpha N+1}^N C_{\text{NL}} \right\}. \quad (43)$$

Since  $R$  is independent of  $\rho_k$ , we should set  $\rho_k \rightarrow 1$  for all  $k = \alpha N + 1, \dots, N$ . Thus, the OPS scheme with

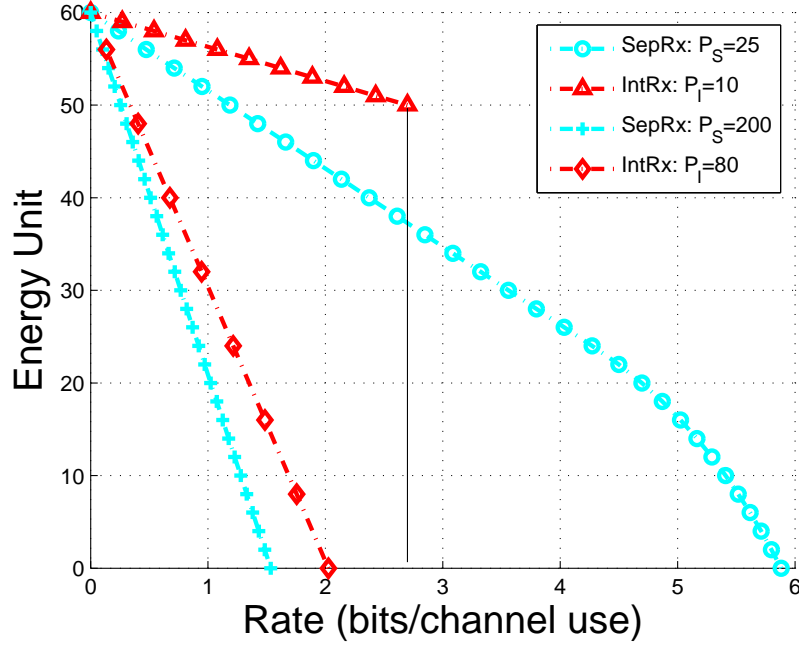


Fig. 10. Rate-energy tradeoff for separated vs. integrated receivers with receiver circuit power consumption. It is assumed that  $h = 1$ ,  $P = 100$ ,  $\zeta = 0.6$ ,  $\sigma_A^2 = 0.01$ ,  $\sigma_{\text{cov}}^2 = 1$  and  $\sigma_{\text{rec}} = 10$ .

$\rho \rightarrow 1$  is the optimal DPS scheme for the integrated receiver with  $P_I > 0$ . Then (44) can be simplified as

$$\mathcal{C}_{\text{R-E}}^{\text{OPS}'}(P) \triangleq \bigcup_{\alpha} \{(R, Q) : Q \leq \zeta h P - (1 - \alpha)P_I, \quad R \leq (1 - \alpha)C_{\text{NL}}\}. \quad (44)$$

Note that when  $P_I < \zeta h P$ , the boundary of  $\mathcal{C}_{\text{R-E}}^{\text{OPS}'}(P)$  is determined by two lines as  $\alpha$  sweeps from 0 to 1, with one vertical line connecting the two points  $(C_{\text{NL}}, 0)$  and  $(C_{\text{NL}}, \zeta h P - P_I)$ , and another line connecting the two points  $(C_{\text{NL}}, \zeta h P - P_I)$  and  $(0, \zeta h P)$ . While  $P_I \geq \zeta h P$ , the boundary of  $\mathcal{C}_{\text{R-E}}^{\text{OPS}'}(P)$  is simply a straight line connecting the two points  $(\zeta h P C_{\text{NL}} / P_I)$  and  $(0, \zeta h P)$  as  $\alpha$  sweeps from  $1 - \zeta h P / P_I$  to 1.

Fig. 10 shows the achievable R-E regions for both cases of SepRx and IntRx with receiver circuit power consumption. We consider two setups for the receiver circuit power consumption, i.e., low circuit power with  $P_S = 25$ ,  $P_I = 10$ , and high circuit power with  $P_S = 200$ ,  $P_I = 80$ . For the low circuit power with  $P_S = 25$ ,  $P_I = 10$ , IntRx is superior over that by SepRx when more harvested power is desired, while SepRx is superior when less harvested power (no greater than 10 energy units) is required. For the high circuit power with  $P_S = 200$ ,  $P_I = 80$ , IntRx is always superior over that by SepRx, since for SepRx much more transmission time needs to be allocated for harvesting energy to compensate the power consumed by information decoding.

## VII. PRACTICAL MODULATION

In this section, we study the performances for the two types of receivers under a realistic system setup that employs practical modulation. Let the signal set (constellation) be denoted by  $\mathcal{X}$ . The size of  $\mathcal{X}$  is denoted by  $M$  with  $M = 2^l$ , and  $l \geq 1$  being an integer. It is assumed that the maximum rate that the practical modulation can support is  $l \leq 10$  bits/channel use. The  $i$ -th constellation point in  $\mathcal{X}$  is denoted by  $x_i, i = 1, \dots, M$ , with equal probability  $p_X(x_i) = 1/M$  for simplicity. For the separated receiver, we assume that coherent  $M$ -ary quadrature amplitude modulation (QAM) is utilized for transmission. The symbol error rate (SER), denoted by  $P_s^{\text{QAM}}$ , is approximated by [20]

$$P_s^{\text{QAM}} \approx \frac{4(\sqrt{M} - 1)}{\sqrt{M}} \mathcal{Q} \left( \sqrt{\frac{3\tau_s}{M - 1}} \right) \quad (45)$$

where  $\tau_s$  denotes the average SNR per symbol at the information receiver<sup>3</sup>. The approximation is tight at high SNR, and is taken to be exact for simplicity in the sequel. For the integrated receiver, as mentioned earlier in Section V, information is encoded by the energy (power) of the transmitted signal. Similar to the pulse amplitude modulation (PAM), we assume a constellation form called *pulse energy modulation* (PEM), with equispaced *positive* constellation points given by

$$x_i = \frac{2(i - 1)}{M - 1}, \quad i = 1, \dots, M. \quad (46)$$

A closed-form expression for the symbol error rate  $P_s^{\text{PEM}}$  appears intractable, due to the coupled antenna and rectifier noise for the channel (26). For most practical systems, the rectifier noise power will be much greater than the antenna noise power, while the antenna noise is approximately at the thermal noise level. This justifies the assumption that  $\sigma_A^2 \ll \sigma_{\text{rec}}$  and we thus approximate the channel (26) with (27). For simplicity, the decision boundary is chosen as the perpendicular bisector of each pair of adjacent two points, and the symbol error rate can be derived to be

$$P_s^{\text{PEM}} = \frac{2(M - 1)}{M} \mathcal{Q} \left( \frac{\tau'_s}{M - 1} \right) \quad (47)$$

where  $\tau'_s = hP/\sigma_{\text{rec}}$  is defined as the average SNR per symbol at the information receiver.

For both separated and integrated receivers, we assume the transmitter can adapt the transmission rate such that the symbol error rate is less than a target value  $P_s^{\text{tgt}}$ , i.e.,  $P_s^{\text{QAM}} \leq P_s^{\text{tgt}}$  and  $P_s^{\text{PEM}} \leq P_s^{\text{tgt}}$  for the separated and

<sup>3</sup>Binary phase shift keying (BPSK) is used when  $l = 1$ . For simplicity, we use (45) to approximate the SER of BPSK at high SNR.

integrated receivers, respectively. Moreover, we assume that there is a minimum net harvested energy requirement  $Q_{\text{req}}$  at the receiver side, i.e.,  $Q \geq Q_{\text{req}}$ , where  $Q_{\text{req}}$  can be used, for example, to power additional sensor components or to be stored in the battery for future use. With the SER constraint and minimum harvested energy constraint, our objective is to achieve the maximum rate. For the separated receiver with OPS scheme, the maximum achievable rate can be obtained by

$$\begin{aligned} \text{(P1)} : \quad & \max_{\alpha, \rho, M} R = (1 - \alpha) \log_2 M \\ \text{s.t.} \quad & \frac{4(\sqrt{M} - 1)}{\sqrt{M}} \mathcal{Q} \left( \sqrt{\frac{3}{M-1} \cdot \frac{(1-\rho)hP}{(1-\rho)\sigma_A^2 + \sigma_{\text{cov}}^2}} \right) \leq P_s^{\text{tgt}}, \end{aligned} \quad (48)$$

$$\alpha \zeta hP + (1 - \alpha) \rho \zeta hP - (1 - \alpha) P_S \geq Q_{\text{req}}, \quad (49)$$

$$0 \leq \alpha \leq 1, \quad 0 \leq \rho \leq 1,$$

$$M = 2^l, \quad l \in \{1, 2, \dots, 10\}$$

Here, the optimization variables are the power splitting pair  $(\alpha, \rho)$  and the modulation size  $M$ .

For the integrated receiver with OPS scheme, the maximum achievable rate can be obtained by

$$\begin{aligned} \text{(P2)} : \quad & \max_{\alpha, M} R = (1 - \alpha) \log_2 M \\ \text{s.t.} \quad & \frac{2(M-1)}{M} \mathcal{Q} \left( \frac{1}{M-1} \cdot \frac{hP}{\sigma_{\text{rec}}} \right) \leq P_s^{\text{tgt}}, \end{aligned} \quad (50)$$

$$\zeta hP - (1 - \alpha) P_1 \geq Q_{\text{req}},$$

$$0 \leq \alpha \leq 1,$$

$$M = 2^l, \quad l \in \{1, 2, \dots, 10\}$$

Note that here the optimization variables only include  $\alpha$  and  $M$ , since the OPS scheme with  $\rho \rightarrow 1$  is optimal for the integrated receiver (c.f. Section VI).

We denote the maximum rate for (P1) and (P2) as  $R_1^*$  and  $R_2^*$ , respectively. Similarly, the optimal variables for (P1) and (P2) are denoted with corresponding superscripts and subscripts, e.g.,  $\alpha_1^*, \rho_1^*$ , etc. Note that both (P1) and (P2) are infeasible when  $Q_{\text{req}}$  is larger than  $\zeta hP$ , which is the maximum possible harvested power by the receivers. With  $Q_{\text{req}} \leq \zeta hP$  and reasonable SNR (such that the SER constraints can be satisfied by some  $M$ ), the optimal solution for (P1) is obtained by an exhaustive search for  $\rho_1^*$ : for each fixed  $\rho_1 \in [0, 1)$ , we



have  $R_1^* = (1 - \alpha_1^*) \log_2 M_1^*$ , where  $\alpha_1^* = \left[ \frac{Q_{\text{req}} - \rho_1 \zeta h P + P_S}{(1 - \rho_1) \zeta h P + P_S} \right]^+$  and  $M_1^*$  attains the maximum value under the SER constraint (48); the optimal  $\rho_1^*$  is then obtained to maximize  $R_1^*$ . The optimal solution for (P2) is given by  $R_2^* = (1 - \alpha_2^*) \log_2 M_2^*$ , where  $\alpha_2^* = \left[ \frac{Q_{\text{req}} - \zeta h P + P_1}{P_1} \right]^+$  and  $M_2^*$  is maximized under the SER constraint (50). For both (P1) and (P2), the achievable rate  $R$  is determined by both the modulation size  $M$  and the time percentage  $\alpha$  that the information decoder operates in the off mode. Moreover, as the received signal power  $hP$  decreases,  $M$  decreases to satisfy the modulation constraint and  $\alpha$  increases to satisfy the harvested energy constraint, both of which result in a decrease of the achievable rate.

Typically for practical systems we have  $P_S > P_1 > 0$ , since the RF band mixer in the separated receiver will consume additional circuit power. Henceforth, we assume  $P_S > P_1 > 0$ .

**Proposition 7.1:** For separated and integrated receivers with  $0 \leq Q_{\text{req}} \leq \zeta h P$  and  $P_S \geq P_1 > 0$ , we have  $\alpha_1^* \geq \alpha_2^*$ . Moreover, if  $M_1^* \leq M_2^*$ , then the maximum achievable rate by the separated receiver will be no greater than that by the integrated receiver, i.e.,  $R_1^* \leq R_2^*$ .

*Proof:* Please refer to Appendix D. ■

Most practical systems of interest typically operate at the high SNR regime for the information receiver, due to the high-power operating requirement for the energy receiver. Thus, for sufficiently small transmission distance, it is expected that both receivers can support the maximum modulation size under the SER constraint, i.e.,  $M_1^* = M_2^* = 2^{10}$ . Thus, by Proposition 7.1, the integrated receiver outperforms the separated receiver for sufficiently small transmission distance.

Fig. 11 shows an example of the maximum achievable rate for a practical point-to-point wireless system with separated or integrated receiver. The corresponding modulation size  $M$  and time percentage  $\alpha$  are shown in Fig. 12. The transmitter power is assumed to be  $P = 1$  watt(W) or 30dBm. The distance from the transmitter to the receiver is assumed to be  $d$  meters with  $d \geq 1$ , which results in approximately  $(-30 - 30 \log_{10} d)$ dB of signal power attenuation at a carrier frequency assumed as  $f_c = 900$ MHz. The bandwidth of the transmitted signal is assumed to be 10MHz. For information receiver, the antenna noise temperature is assumed to be 290K, which corresponds to  $\sigma_A^2 = -104$ dBm over the bandwidth of 10MHz. As in most practical wireless communication systems, it is assumed that the processing noise power is much greater than the antenna noise power, in which

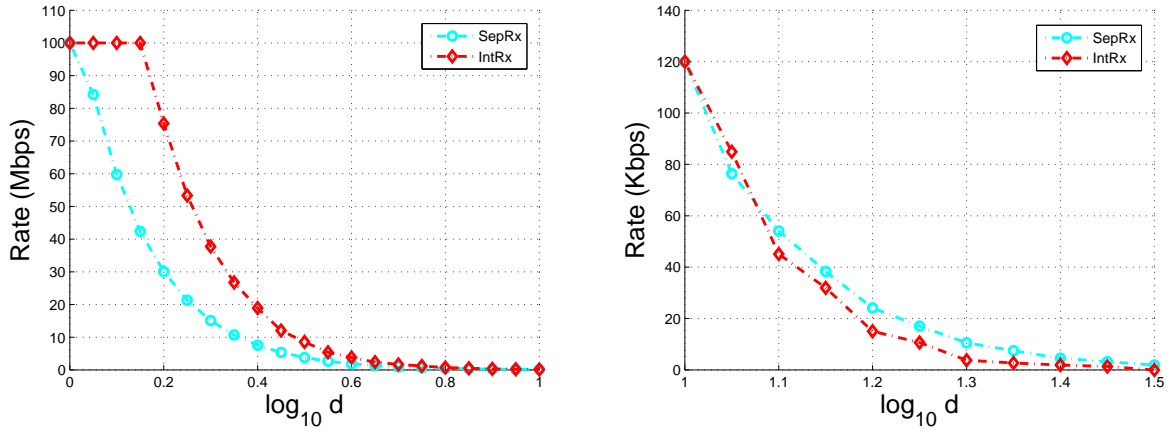


Fig. 11. Maximum achievable rate for separated and integrated receivers over different transmission distance.

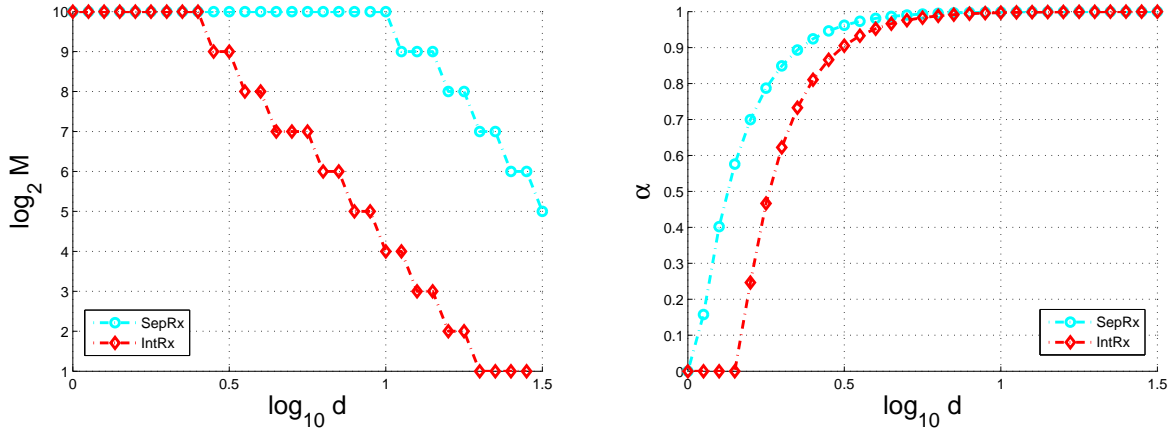


Fig. 12. Optimal modulation size ( $M$ ) and information receiver off-time percentage ( $\alpha$ ) for separated and integrated receivers.

case the antenna noise can be omitted. In particular, it is assumed that  $\sigma_{\text{cov}}^2 = -70\text{dBm}$  for the separated receiver and  $\sigma_{\text{rec}} = -50\text{dBm}$  for the integrated receiver. The circuit power consumed by information decoding is assumed to be  $P_S = 0.5\text{mW}$  for the separated receiver, and  $P_I = 0.2\text{mW}$  for the integrated receiver. For energy receiver, the energy conversion efficiency is assumed to be  $\zeta = 60\%$ . The minimum harvested energy requirement  $Q_{\text{req}}$  is set to be zero, which is the minimum requirement for a zero-net-energy system that does not need external power source. The symbol error rate target is assumed to be  $P_s^{\text{tgt}} = 10^{-5}$ .

In Fig. 11, it is observed that when  $0 \leq \log_{10} d \leq 1$ , IntRx achieves more rate than SepRx. By Proposition 7.1, IntRx outperforms SepRx over the range  $0 \leq \log_{10} d \leq 0.4$  with  $M_1^* = M_2^* = 2^{10}$ ; however, Proposition 7.1 provides only a sufficient condition, numerical results show that IntRx outperforms SepRx over longer distances up to  $\log_{10} d \leq 1$ . This is due to the fact that although SepRx supports higher-order constellations (larger  $M$ )

than IntRx when  $0.4 < \log_{10} d \leq 1$ , the information receiver of SepRx needs to operate in the off mode for more time (larger  $\alpha$ ) to compensate the power consumed by information decoding (c.f. Fig. 12). It turns out that over this range, the average rate over the whole transmission time of SepRx is less than that achieved by IntRx. As  $\log_{10} d$  increases, the rate gap between SepRx and IntRx shrinks and converges when  $\log_{10} d = 1$ . When  $1.1 \leq \log_{10} d \leq 1.5$ , SepRx achieves more rate than IntRx, since  $\alpha$  for both receivers approaches to 1 (c.f. Fig. 12), while the achievable rates are dominated by the modulation size ( $M$ , c.f. Fig. 12). Note that when  $\log_{10} d = 1.5$ , no modulation can support IntRx due to the extremely low received SNR; however, SepRx can still achieve some positive rate. In addition, Fig. 12 shows that in general IntRx exploits lower complexity (smaller  $M$ ) in generating signal constellation.

## VIII. CONCLUSION

This paper investigates practical receiver designs for wireless simultaneous information and power transfer. Based on *dynamic power splitting* (DPS), we propose two practical receiver architectures, namely, *separated* versus *integrated* information and energy receivers. For the separated receiver, the received signal by the antenna is split into two signal streams in the RF band, which are then separately fed to the conventional energy receiver and information receiver for harvesting energy and decoding information, respectively. For the integrated receiver, part of the information decoding implementation, i.e., the RF to baseband conversion, is integrated to the energy receiver via the rectifier. For both receivers, we characterize the rate-energy performance taking circuit power consumption into account. Numerical results show that when the circuit power consumptions are small (compared with the received signal power), the separated receiver is superior at low harvested power region; while the integrated receiver performs better at high harvested power region. When the circuit power consumptions are large, the integrated receiver is superior than separated receiver. Moreover, the performance for the two types of receivers is studied under a realistic system setup that employs practical modulation. With symbol error rate constraint and minimum harvested power constraint, the maximum achievable rates by the two types of receivers are compared. It is shown that for a system with zero-net-energy consumption, the integrated receiver achieves more rate than separated receiver at small transmission distances.

## APPENDIX A

## PROOF OF PROPOSITION 4.1

To show  $\mathcal{C}_{\text{R-E}}^{\text{DPS}}(P) = \mathcal{C}_{\text{R-E}}^{\text{SPS}}(P), \forall P \geq 0$ , it suffices for us to show that  $\mathcal{C}_{\text{R-E}}^{\text{SPS}}(P) \subseteq \mathcal{C}_{\text{R-E}}^{\text{DPS}}(P), \forall P \geq 0$  and  $\mathcal{C}_{\text{R-E}}^{\text{DPS}}(P) \subseteq \mathcal{C}_{\text{R-E}}^{\text{SPS}}(P), \forall P \geq 0$ . The first part of proof is trivial, since SPS is just a special case of DPS by letting  $\rho_k = \rho, \forall k$  (c.f. (17)). Next, we prove the second part. Assuming that  $f(\rho) = \log_2 \left( 1 + \frac{(1-\rho)hP}{(1-\rho)\sigma_A^2 + \sigma_{\text{cov}}^2} \right)$ , it is easy to verify that  $f(\rho)$  is concave in  $\rho \in [0, 1]$ . By Jensen's inequality, we have  $\frac{1}{N} \sum_{k=1}^N f(\rho_k) \leq f\left(\frac{1}{N} \sum_{k=1}^N \rho_k\right)$ . Thus, for  $\forall \boldsymbol{\rho} = [\rho_1, \dots, \rho_N]^T$ ,  $\exists \rho = \frac{1}{N} \sum_{k=1}^N \rho_k$ , so that  $\frac{1}{N} \sum_{k=1}^N \rho_k \zeta hP = \rho \zeta hP$  and  $\frac{1}{N} \sum_{k=1}^N f(\rho_k) \leq f(\rho)$ . Since R-E region is defined as the union of rate-energy pairs  $(R, Q)$  under all possible  $\boldsymbol{\rho}$ , it follows immediately that  $\mathcal{C}_{\text{R-E}}^{\text{DPS}}(P) \subseteq \mathcal{C}_{\text{R-E}}^{\text{SPS}}(P), \forall P \geq 0$ , which completes the proof of Proposition 4.1.

## APPENDIX B

## PROOF OF PROPOSITION 6.1

To show  $\mathcal{C}_{\text{R-E}}^{\text{DPS}'}(P) = \mathcal{C}_{\text{R-E}}^{\text{OPS}'}(P), \forall P \geq 0$ , it suffices for us to show that  $\mathcal{C}_{\text{R-E}}^{\text{OPS}'}(P) \subseteq \mathcal{C}_{\text{R-E}}^{\text{DPS}'}(P), \forall P \geq 0$  and  $\mathcal{C}_{\text{R-E}}^{\text{DPS}'}(P) \subseteq \mathcal{C}_{\text{R-E}}^{\text{OPS}'}(P), \forall P \geq 0$ . The first part of proof is trivial, since OPS is just a special case of DPS by letting  $\rho_k = \rho, k = \alpha N, \dots, N$  (c.f. (18)). Next, we prove the second part. By (35),  $\rho_k$ 's are optimized at  $\rho_k = 1$  for  $k = 1, \dots, \alpha N$ ; thus, we have  $Q \leq \alpha \zeta hP + \frac{1}{N} \sum_{k=\alpha N+1}^N \rho_k \zeta hP - (1-\alpha)P_S$  for DPS. For any given  $\alpha$ , by Jensen's inequality we have  $\frac{1}{(1-\alpha)N} \sum_{k=\alpha N+1}^N f(\rho_k) \leq f\left(\frac{1}{(1-\alpha)N} \sum_{k=\alpha N+1}^N \rho_k\right)$ . Thus, for  $\forall \alpha$  and  $\forall \boldsymbol{\rho} = [\rho_1, \dots, \rho_N]^T$ ,  $\exists \rho = \frac{1}{(1-\alpha)N} \sum_{k=\alpha N+1}^N \rho_k$ , so that  $\frac{1}{N} \sum_{k=\alpha N+1}^N \rho_k \zeta hP = (1-\alpha)\rho \zeta hP$  and  $\frac{1}{N} \sum_{k=\alpha N+1}^N f(\rho_k) \leq (1-\alpha)f(\rho)$ . Since R-E region is defined as the union of rate-energy pairs  $(R, Q)$  under all possible  $\boldsymbol{\rho}$ , it follows immediately that  $\mathcal{C}_{\text{R-E}}^{\text{DPS}'}(P) \subseteq \mathcal{C}_{\text{R-E}}^{\text{OPS}'}(P), \forall P \geq 0$ , which completes the proof of Proposition 6.1.

## APPENDIX C

## PROOF OF LEMMA 6.1

From (41), the first and second derivatives of  $R(s)$  with respect of  $s$  are given by

$$\frac{dR}{ds} = \log_2 \left( 1 + \frac{cs+d}{as+b} \right) + \frac{s(bc-ad)}{((a+c)s+b+d)(as+b)\ln 2}, \quad (51)$$

$$\frac{d^2R}{ds^2} = \frac{(bc-ad)((b(a+c)+a(d+d))s+2b(d+d))}{((a+c)s+b+d)^2(as+b)^2\ln 2}. \quad (52)$$

From (52), the sign of  $\frac{d^2 R}{ds^2}$  is identical with the line  $f_2(s) = (bc - ad)((b(a + c) + a(d + d))s + 2b(d + d))$ . Note that  $bc - ad = -\sigma_{\text{cov}}^2(hP - Q/\zeta) \leq 0$ ,  $f_2(0) = 2b(b + d)(bc - ad) \leq 0$ , and  $f_2(-\frac{d}{c}) = \frac{(2b+d)(bc-ad)^2}{c} \leq 0$ , thus we have  $\frac{d^2 R}{ds^2} \leq 0$  for  $s \in [0, -\frac{d}{c}]$ , which proves that  $R(s)$  is concave in  $s \in [0, -\frac{d}{c}]$ . Moreover, from (51), we have  $\frac{dR}{ds}|_{s=0} = \log_2(1 + b/d) > 0$  and  $\frac{dR}{ds}|_{s=-d/c} = \frac{d(bc-ad)}{-c(-ad/c+b)^2} < 0$ . Thus, as  $s$  increases from 0 to  $-\frac{d}{c}$ ,  $R(s)$  decreases after an initial increase, which completes the proof of Lemma 6.1.

## APPENDIX D

### PROOF OF PROPOSITION 7.1

We first consider (P1) with  $0 \leq Q_{\text{req}} \leq \zeta hP$  for the separated receiver. The optimal  $\alpha$  for (P1) is given by  $\alpha_1^* = \left[ \frac{Q_{\text{req}} - \rho_1^* \zeta hP + P_S}{(1 - \rho_1^*) \zeta hP + P_S} \right]^+$ . Since  $Q_{\text{req}} \leq \zeta hP$ ,  $\alpha_1^*$  decreases as  $\rho_1^*$  increases. Thus, we have

$$\alpha_1^* \geq \frac{Q_{\text{req}} - \rho_1^* \zeta hP + P_S}{(1 - \rho_1^*) \zeta hP + P_S} \Big|_{\rho_1^*=1} = \frac{Q_{\text{req}} - \zeta hP + P_S}{P_S}. \quad (53)$$

Next, for the integrated receiver with  $0 \leq Q_{\text{req}} \leq \zeta hP$ , the optimal  $\alpha$  for (P2) is given by

$$\alpha_2^* = \left[ \frac{Q_{\text{req}} - \zeta hP + P_1}{P_1} \right]^+ \quad (54)$$

From (53) and (54), we have  $\alpha_1^* \geq \alpha_2^*$ , given that  $P_S > P_1$ . Since  $R = (1 - \alpha) \log_2 M$ , we have  $R_1^* \leq R_2^*$ , given that  $\alpha_1^* \geq \alpha_2^*$  and  $M_1^* \leq M_2^*$ . The proof of Proposition 7.1 thus follows.

## REFERENCES

- [1] L. R. Varshney, "Transporting information and energy simultaneously," in *Proc. IEEE Int. Symp. Inf. Theory (ISIT)*, pp. 1612-1616, July 2008.
- [2] P. Grover and A. Sahai, "Shannon meets Tesla: wireless information and power transfer," in *Proc. IEEE Int. Symp. Inf. Theory (ISIT)*, pp. 2363-2367, June 2010.
- [3] L. Liu, R. Zhang, and K. C. Chua, "Wireless information transfer with opportunistic energy harvesting," *IEEE Trans. Wireless Commun.*, accepted for publication. Available online at [arXiv:1204.2035].
- [4] R. Zhang and C. K. Ho, "MIMO broadcasting for simultaneous wireless information and power transfer," in *Proc. IEEE Globecom*, Dec. 2011.
- [5] Z. Xiang and M. Tao, "Robust beamforming for wireless information and power transmission," *IEEE Wireless Commun. Letters*, vol. 1, no. 4, pp. 372-375, 2012.
- [6] B. K. Chalise, Y. D. Zhang, and M. G. Amin, "Energy harvesting in an OSTBC based amplify-and-forward MIMO relay system," in *Proc. IEEE ICASSP*, pp. 3201-3204, Mar. 2012.
- [7] A. M. Fouladgar and O. Simeone, "On the transfer of information and energy in multi-user systems," *IEEE Commun. Letters*, accepted for publication.
- [8] K. Huang and V. K. N. Lau, "Enabling wireless power transfer in cellular networks: architecture, modeling and deployment," Available on-line at [arXiv:1207.5640].

- [9] S. Lee, K. Huang, and R. Zhang, "Cognitive energy harvesting and transmission from a network perspective," Available on-line at [arXiv:1209.3505].
- [10] T. Cover and J. Thomas, *Elements of information theory*, New York: Wiley, 1991.
- [11] T. Paing, J. Shin, R. Zane, and Z. Popovic, "Resistor emulation approach to low-power RF energy harvesting," *IEEE Trans. Power Electronics*, vol. 23, no. 3, pp. 1494-1501, May 2008.
- [12] J. A. G. Akkermans, M. C. van Beurden, G. J. N. Doodeman, and H. J. Visser, "Analytical models for low-power rectenna design," *IEEE Antennas Wireless Propag. Letters*, vol. 4, pp. 187-190, 2005.
- [13] Product Datasheet, P2110-915MHz RF Powerharvester Receiver, Powercast Corporation.
- [14] H. Urkowitz, "Energy detection of unknown deterministic signals," *Proc. IEEE*, vol. 55, pp. 523-231, Apr. 1967.
- [15] A. A. Farid and S. Hranilovic, "Upper and lower bounds on the capacity of wireless optical intensity channels," in *Proc. IEEE Int. Symp. Inf. Theory (ISIT)*, pp. 2416-2420, June 2007.
- [16] I. Abou-Faycal and J. Fahs, "On the capacity of some deterministic non-linear channels subject to additive white Gaussian noise," in *Proc. IEEE Int. Conf. on Telecommunications (ICT)*, pp. 63-70, Apr. 2010.
- [17] A. Lapidoth, S. M. Moser, and M. A. Wigger, "On the capacity of free-space optical intensity channels," *IEEE Trans. Inf. Theory*, vol. 55, no. 10, pp. 4449-4461, Oct. 2009.
- [18] M. Katz and S. Shamai (Shitz), "On the capacity-achieving distribution of the discrete-time noncoherent and partially coherent AWGN channels," *IEEE Trans. Inf. Theory*, vol. 50, no. 10, pp. 2257-2270, Oct. 2004.
- [19] A. Lapidoth, "On phase noise channels at high SNR," in *Proc. IEEE Inf. Theory Workshop (ITW)*, Oct. 2002.
- [20] A. Goldsmith, *Wireless communications*, Cambridge University Press, 2005.